

Sideband Transitions and Two-Tone Spectroscopy of a Superconducting Qubit Strongly Coupled to an On-Chip Cavity

A. Wallraff^{*}, D. I. Schuster, A. Blais[†], J. M. Gambetta, J. Schreier,
L. Frunzio, M. H. Devoret, S. M. Girvin, and R. J. Schoelkopf
Departments of Applied Physics and Physics, Yale University, New Haven, CT 06520
(Dated: April 15, 2004)

Sideband transitions are spectroscopically probed in a system consisting of a Cooper pair box strongly but non-resonantly coupled to a superconducting transmission line resonator. When the Cooper pair box is operated at the optimal charge bias point the symmetry of the hamiltonian requires a two-photon process to access sidebands. The observed large dispersive ac-Stark shifts in the sideband transitions induced by the strong non-resonant drives agree well with our theoretical predictions. Sideband transitions are important in realizing qubit-photon and qubit-qubit entanglement in the circuit quantum electrodynamics architecture for quantum information processing.

A promising route towards the implementation of a scalable solid state quantum information processor [1] is based on superconducting quantum electronic circuits. The basic concepts of creating coherent quantum two-level systems (qubits) from superconducting circuit elements such as inductors, capacitors and Josephson junctions (an ideal, non-linear inductor) are well understood [2] and a variety of qubits have been implemented in a wide range of architectures [3]. The realization of controlled qubit interactions [4, 5, 6, 7, 8] and the implementation and characterization of two-qubit gate operations [9, 10] is a main objective of current research. Many implementations are, however, limited to static nearest neighbor couplings. By coupling individual qubits to a common harmonic oscillator mode used as a bus [11, 12, 13] non-local interactions can be mediated between very distant qubits, a much more versatile and scalable approach for quantum information processing.

A promising realization of such a system is based on a set of Cooper pair boxes strongly coupled to a high quality transmission line resonator [12]. In this circuit quantum electrodynamics (QED) architecture [12], it has been demonstrated spectroscopically that a single photon can be exchanged coherently between a superconducting cavity and an individual qubit [14] in a resonant process known as the vacuum Rabi mode splitting. This resonant process has also been observed as time-resolved oscillations in a persistent current qubit coupled to a lumped element oscillator [7, 16]. This feat is essential for non-local qubit coupling and for quantum communication as it allows to transfer quantum information from stationary qubits to photons used as 'flying' qubits that may enable hybrid quantum information systems [17].

In the circuit QED architecture high fidelity qubit control has been demonstrated and the strong non-resonant (or dispersive) coupling of individual qubits to cavity photons has been successfully employed for high visibility readout of the qubit state [18, 19]. In the dispersive regime, when the transition frequency ω_a between the qubit ground state $|g\rangle$ and excited state $|e\rangle$ is detuned

by an amount $\delta = \omega_a - \omega_r$ from the cavity frequency ω_r , the resonant qubit-photon interaction is suppressed. Nevertheless, sideband transitions, see Fig. 1a, may be used to transfer a qubit state to a photon state, also see Ref. [15]. Sideband transitions are induced by driving the coupled qubit-cavity system at its sum $\omega_{blue} = \omega_a + \omega_r$ (blue sideband) or difference frequencies $\omega_{red} = \omega_a - \omega_r$ (red sideband). Similarly sidebands have been accessed in a system in which a qubit is coupled to a SQUID oscillator also used for readout [7]. Using such sideband transitions, entanglement between a qubit and the resonator could potentially be generated, a process essential for realizing non-local gate operations in a set of qubits

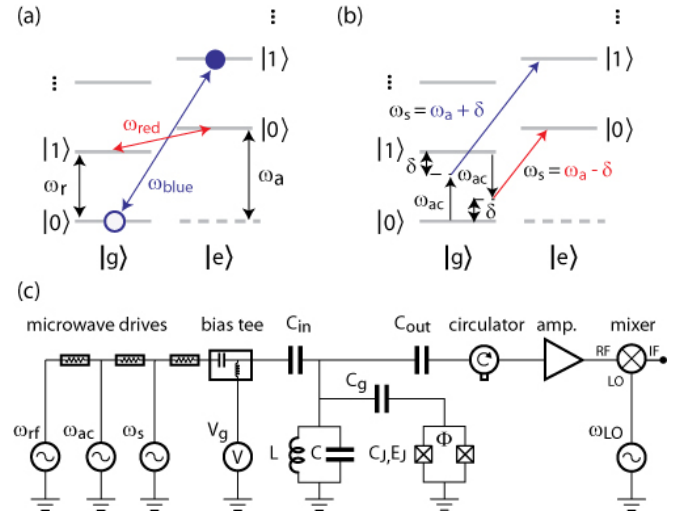


FIG. 1: (color online) (a) Dispersive dressed states energy level diagram for qubit states $|g\rangle$ and $|e\rangle$ with separation ω_a and single mode cavity photon states $|j\rangle = |0\rangle, |1\rangle, |2\rangle, \dots$ with separation ω_r . Red (ω_{red}) and blue (ω_{blue}) sideband transitions are indicated. (b) Two-tone scheme for sideband transitions. Fixed ac-tone ω_{ac} detuned by δ from cavity combined with spectroscopy tone $\omega_s = \omega_a$ induces sideband transitions. (c) Measurement setup for two-tone spectroscopy, compare with setups in Refs. [14, 19]. An extra phase coherent microwave source at the ac-tone is applied to the cavity input.

coupled to a cavity.

In this letter, we demonstrate an approach to access the red and blue sideband transitions of a Cooper pair box biased at its optimal point and coupled to a cavity using two microwave tones at different frequencies. We spectroscopically probe the sideband transitions and explain the observed transition frequencies induced by two independent non-resonant drives.

We consider a Cooper pair box [20] with Josephson energy $E_{J\text{max}} = 12 \text{ GHz}$ and single electron charging energy $E_c = 4.75 \text{ GHz}$ biased at its optimal point [21] as an ideal two-level system with a ground state $|j_i\rangle$, an excited state $|j_e\rangle$ and bare transition frequency $\nu_a = 5.8 \text{ GHz}$. The Cooper pair box is coupled with strength $g = 17 \text{ MHz}$ to a harmonic oscillator with states $|j_i\rangle, |j_i+1\rangle, \dots, |j_i\rangle$ realized as a single mode of a transmission line resonator [22] with frequency $\nu_r = 5.5 \text{ GHz}$ and decay rate $\gamma = 0.5 \text{ MHz}$. The strong coupling limit of cavity QED is realized in this system [14] and its dynamics are described by the Jaynes-Cummings Hamiltonian [12]. Using applied magnetic flux, the split Cooper pair box is detuned from the cavity by $\nu_a - \nu_r = 2350 \text{ MHz}$ g.

The qubit transition frequency $\nu_a = 5.877 \text{ GHz}$ is found by applying a spectroscopy microwave tone at frequency ν_s to the cavity and measuring the phase shift of a microwave beam applied to the system at the cavity frequency ν_r , as demonstrated in Ref. 18. Using this single frequency scheme however, the red and blue sidebands cannot be observed because the single photon transitions are to first order forbidden when the Cooper pair box is biased at charge degeneracy. This can be seen by introducing the parity operator $P = e^{i\pi a^\dagger a}$ and recognizing that states involved in the sideband transitions are of equal parity while the term in the Hamiltonian responsible to drive these transitions is of odd parity [13, 15, 23]. Away from charge degeneracy, the sideband transitions are allowed, but at the expense of

reduced coherence times due to the larger sensitivity of the qubit to charge noise [24].

Going to second order in the drive Hamiltonian, the above considerations mean that two-photon sideband transitions are allowed at charge degeneracy. One way to drive these two-photon transitions is simply to choose the drive frequency to be $\nu_{\text{red/blue}} = 2\nu_s$. The red sideband, however, is strongly detuned from the resonator and it is difficult to drive the transition at the required rate because of the filtering due to the cavity at large detunings, also see Fig. 2.

As a result, here, we choose to drive sideband transitions at charge degeneracy with two photons of frequencies ν_{ac} and ν_s that can be selected freely with the constraint that their sum or difference must match the desired sideband $\nu_{\text{red/blue}} = \nu_{ac} \pm \nu_s$. In particular, an on-resonant ac-Stark drive at fixed frequency $\nu_{ac} = \nu_r$ is chosen at a small detuning from the cavity frequency, see Fig. 1b. The power coupled into the cavity for a fixed external drive scales as $1/\nu_{ac}^2$ and thus is largest for small values of ν_{ac} . A second microwave drive applied at frequency $\nu_s = \nu_a - \nu_{ac}$ then induces two-photon blue or red sideband transitions, respectively, as shown in Fig. 1b. The effective Hamiltonians describing these processes are given by [13]

$$H_{2R} = \frac{g}{4} \frac{\nu_{ac}}{\nu_a - \nu_{ac}} \frac{\nu_s}{\nu_a - \nu_s} a^\dagger + a + ; \quad (1)$$

$$H_{2B} = \frac{g}{4} \frac{\nu_{ac}}{\nu_a - \nu_{ac}} \frac{\nu_s}{\nu_a - \nu_s} a^\dagger + a + ;$$

where $\nu_{ac/s}$ are Rabi frequencies given by

$$\nu_{ac/s} = \frac{2g_{ac/s}}{\nu_r - \nu_{ac/s}}; \quad (2)$$

with the drive amplitudes $g_{ac/s}$ expressed as frequencies, also see Eq. (5).

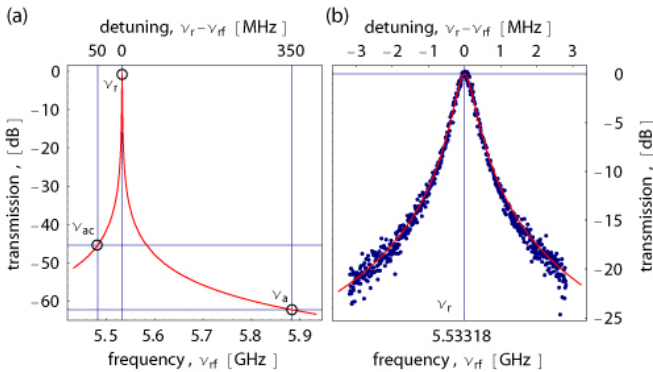


FIG. 2: (color online) (a) Calculated Lorentzian cavity transmission spectrum over large frequency range. The cavity drives at frequencies ν_s , ν_{rf} , ν_r and ν_{ac} and the cavity transmission at these frequencies are indicated. (b) Measured cavity spectrum (dots) and fit (line) around cavity frequency.

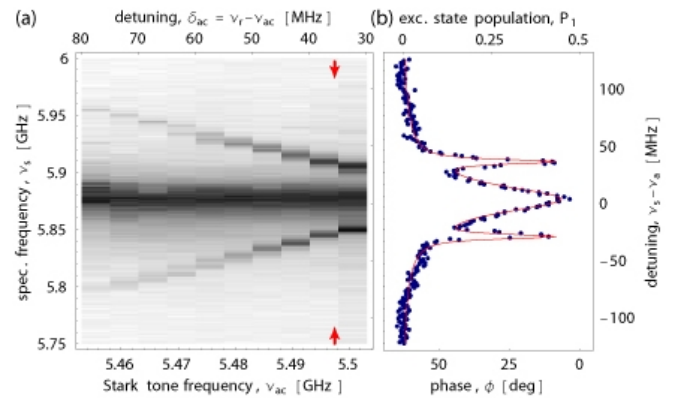


FIG. 3: (color online) (a) Density plot of measured cavity phase shift (white : 70 deg, black : 0 deg) vs. ν_s and ν_{ac} . (b) Measured phase shift vs. ν_s for $\nu_r = 50 \text{ MHz}$ (dots) as indicated by arrows in (a) and fit to linear combination of three independent Lorentzian line shapes (solid line).

Figure 3b shows the cavity phase shift in the presence of a fixed power and fixed frequency ac-Stark tone chosen at a detuning of $\Delta = 2\pi \times 35$ MHz in response to a spectroscopic drive scanned around the qubit transition frequency. The main qubit transition at ν_a and the two sidebands at ν_{\pm} are clearly observed. We also note that the sideband transitions can be saturated at suitably chosen drive powers indicating that sideband oscillations should be observable in future experiments. In Fig. 3a, the sideband transitions are shown varying the detuning but keeping the drive amplitudes fixed. In this parameter range, the sideband frequencies scale as expected to first order linearly with the detuning and the amplitudes of the peaks decrease with detuning as the effective photon number in the cavity decreases with Δ due to the cavity filtering.

At higher drive amplitudes, however, large shifts of the sideband frequencies from ν_{\pm} become apparent. In Fig. 4a, the center and sideband transition frequencies are indicated as extracted from the peak positions of Lorentzian line fits, similar to those in Fig. 3b, for an ac-Stark tone power increased by a factor of 4 in comparison to the measurement presented in Fig. 3. This data shows that all transitions are shifted to higher frequen-

cies as the detuning decreases, an effect that can be explained considering the ac-Stark shifts [18] induced in the qubit transition frequency by the off-resonant drives. As both drives at ν_{ac} and ν_s are detuned from the qubit transition by Δ and $\Delta + \nu_s$ they induce dispersive shifts in the qubit frequency

$$\nu_a = \nu_a + \frac{1}{2} \frac{\Omega_{ac}^2}{\Delta \nu_{ac}} + \frac{1}{2} \frac{\Omega_s^2}{\Delta \nu_s}; \quad (3)$$

that depend on the drive strengths $\Omega_{ac,s}$ and frequencies $\nu_{ac,s}$. The shift due to the additional drive used to measure the qubit population is taken into account in the same way [18]. These off-resonance ac-Stark shifts are important at large drive amplitudes, i.e. when the qubit transition is saturated, and small detunings. It is important to note that any frequency multiplexed scheme used to address multiple qubits is affected by such shifts. However, the effect can be compensated for by appropriately readjusting the qubit drive frequencies.

At a fixed ac-Stark tone, the blue and red sideband frequencies are then determined by the nonlinear equation

$$\nu_s = \nu_a \quad (4)$$

for ν_s that allows one to accurately fit the center frequencies of both the fundamental and the sidebands with the same set of parameters, see Fig. 4.

The drive amplitudes required for the fits using Eq. (2) were calibrated using the ac-Stark shift of the qubit transition induced by the measurement beam resonant with the cavity frequency ν_r . At this frequency an input power of $P_{rf}^{(1)} = 28$ dBm corresponds to an average cavity photon occupation number of $n = 1$. The photon number n is related to the drive amplitude

$$n = \frac{2}{2 + (\Delta/2)^2}; \quad (5)$$

depending on the detuning from the cavity and the cavity decay rate γ . Having accurately measured (see Fig. 2b) and knowing γ , the values for Δ are accurately and consistently determined for all fits.

For the sideband measurements presented in Fig. 4b, we have chosen a fixed detuning of $\Delta = 50$ MHz and have varied the ac-Stark tone power over two orders of magnitude and kept the dispersive shifts due to the spectroscopy drive minimal by keeping the drive amplitude low. As observed, the dispersive shifts in the qubit frequency with drive power can be much larger than the qubit line widths and are well described by Eqs. (3-4), see lines in Fig. 4. As the frequencies of the two tones are smaller than both the cavity and the qubit frequency all lines are shifted to higher frequencies, see Eq. (3).

In the case that the spectroscopy drive amplitude dominates the dispersive shifts, the red sideband is shifted to

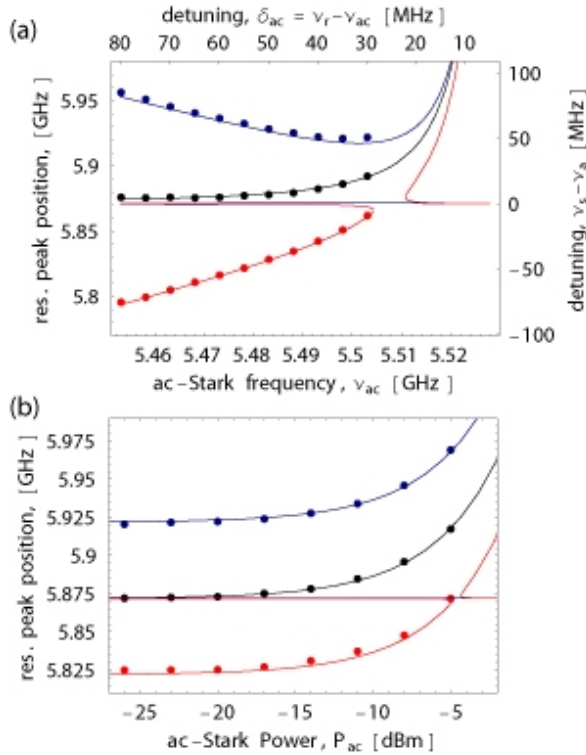


FIG. 4: (color online) (a) Two-tone red and blue sidebands (red/blue dots) and fundamental (black dots) qubit transition frequencies for fixed P_s and P_{ac} varying ν_{ac} . Lines are fits to Eqs. (3-4) (b) For fixed ν_{ac} , and varying P_{ac} . Measurements are done at fixed measurement frequency $\nu_{rf} = \nu_r$ and power P_{rf} weakly populating the resonator with $n_{rf} \approx 2$ photons.

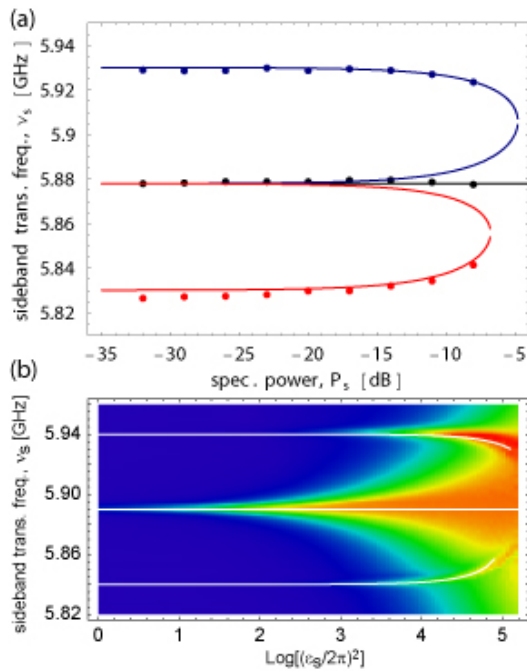


FIG. 5: (color online) (a) As Fig. 4b but for fixed δ_{ac} , P_{ac} and varying P_s . (b) Master equation simulation of the qubit inversion h_{zi} as a function of spectroscopy frequency $\nu_s/2\pi$ and the spectroscopy power $\log(\nu_s/2\pi)^2$ on a logarithmic scale. Blue: $h_{zi} = 1$; Red: $h_{zi} = 0$. The white lines are obtained from Eqs. (3) and (4). The parameter values used in the simulation are those quoted in the text.

higher frequencies, whereas the blue sideband is shifted to lower frequencies, since the detuning of the spectroscopy drive from the bare qubit transition frequency has different signs. This situation is analyzed in Fig. 5, where the spectroscopy power is varied by 3 orders of magnitude at fixed detuning of $\delta = 50$ MHz. Again the sideband transition frequencies are predicted well by our analysis. As shown in Fig. 5b, these results also agree well with numerical simulation of the system's master equation in the Born-Markov approximation [13].

We have demonstrated that sideband transitions can be driven in a Cooper pair box coupled to a transmission line resonator and biased at the optimal point using two photons of different frequencies. Large shifts in the qubit level separation are observed and can be explained and predicted considering the ac-Stark shifts induced by the non-resonant drives. These are particularly important at high drive amplitudes that are required for short pulses that can be potentially used to entangle a qubit with a cavity photon and to generate qubit-qubit entanglement. A protocol for entangling qubits could follow these lines. We would start out with both the cavity and a detuned qubit in their ground state $|j;gi\rangle$ and apply a pulse to the qubit to generate the state $|j;ei\rangle$. With a $\omega_s/2\pi = 2$ red sideband pulse on the coupled system we would generate a maximally entangled cavity-qubit state

of the form $|j;ei\rangle + |j;gi\rangle$. This entanglement would then be transferred to generate a qubit-qubit entangled state. Applying a pulse on the red sideband of a second qubit would prepare a final state of the form $|j;gi\rangle + |j;ei\rangle$, which is a Bell state of two superconducting qubits and leaves the cavity in its ground state and completely unentangled from the qubits. This scheme would be an on-resonant implementation of the generation of entangled qubit pairs inspired by the protocol demonstrated for Rydberg atoms [25] and trapped ions [26]. We also note that single microwave photon sources could be realized and cavity Fock states could be prepared in circuit QED using this sideband scheme.

This work was supported in part by the NSA under ARO contract W 911NF-05-1-0365, and the NSF under ITR 0325580 and DMR-0603369, and the W. M. Keck Foundation. AB was partially supported by NSERC, FQRNT and CIAR.

Department of Physics, ETH Zurich, CH-8093 Zurich, Switzerland

^y Département de Physique et Regroupement Québécois sur les Matériaux de Pointe, Université de Sherbrooke, Sherbrooke, Québec, Canada, J1K 2R1

- [1] M. A. Nielsen and I. L. Chuang, Quantum computation and quantum information (Cambridge University Press, 2000).
- [2] M. H. Devoret, A. Wallraef, and J. M. Martinis, cond-mat/0411174 (2004).
- [3] G. Wendin and V. Shumeiko, cond-mat/0508729 (2005).
- [4] A. J. Berkley et al., Science 300, 1548 (2003).
- [5] Y. A. Pashkin et al., Nature 421, 823 (2003).
- [6] J. B. Majer et al., Phys. Rev. Lett. 94, 090501 (2005).
- [7] I. Chiorescu et al., Nature (London) 431, 159 (2004).
- [8] R. M. McDermott et al., Science 307, 1299 (2005).
- [9] T. Yamamoto et al., Nature 425, 941 (2003).
- [10] M. Steffen et al., Science 313, 1423 (2006).
- [11] Y. Makhlin, G. Schon, and A. Shnirman, Nature 398, 305 (1999).
- [12] A. Blais et al., Phys. Rev. A 69, 062320 (2004).
- [13] A. Blais et al., cond-mat/0612038 (2006).
- [14] A. Wallraef et al., Nature (London) 431, 162 (2004).
- [15] Y. Xi Liu et al., (2005), cond-mat/0509236.
- [16] J. Johansson et al., Phys. Rev. Lett. 96, 127006 (2006).
- [17] A. Andre et al., Nature Physics 2, 636 (2006).
- [18] D. I. Schuster et al., Phys. Rev. Lett. 94, 123602 (2005).
- [19] A. Wallraef et al., Phys. Rev. Lett. 95, 060501 (2005).
- [20] V. Bouchiat et al., Physica Scripta T 76, 165 (1998).
- [21] D. Vion et al., Science 296, 886 (2002).
- [22] L. Frunzio et al., IEEE Trans. Appl. Supercond. 15, 860 (2005).
- [23] Y. Xi Liu et al., Physical Review Letters 95, 087001 (2005).
- [24] G. Ithier et al., et al., Phys. Rev. B 72, 134519 (2005).
- [25] J. Ramond, M. Brune, and S. Haroche, Rev. Mod. Phys. 73, 565 (2001).
- [26] F. Schmidt-Kaler et al., Nature 422, 408 (2003).